Formulation and phase change mechanism of Capric acid/Octadecanol binary composite phase change materials

Peixian Zuo [a], Zhong Liu [a], Hua Zhang [a], Dasong Dai [a,**], Ziyan Fu [b], Jorge Corker [c], Mizi Fan [a,b,*]

[a] College of Materials Engineering; College of Transportation and Civil Engineering, Fujian Agriculture and Forestry University, 350002, Fuzhou, China
[b] College of Engineering, Design and Physical Science, Brunel University London, UB8 3PH, Uxbridge, United Kingdom
[c] IPN Led&mat, Rua Pedro Nunes, 3030 199, Coimbra, Portugal

ARTICLE INFO

ABSTRACT

Fatty acids and fatty alcohols have the advantages of high latent heat of phase change, good thermal stability, no corrosion, no supercooling and phase separation. They can be used as phase change energy storage materials for passive temperature control. However, their popularization and application are limited because of their high phase transition temperature and narrow phase transition range. This study develops a novel binary composite phase change materials (PCMs) of Capric acid (CA) and Octadecanol (OD) by a melt blending method. The theoretical calculation and hot melt-step cooling were carried out to generate an optimal molar ratio, followed by DSC thermal characterization. ATR-FTIR and XRD were performed to determine the phase transformation and chemical and structure changes. The results showed the binary CA-OD binary composite PCMs has a high latent heat of fusion, a melting temperature T_m = 26.48 °C and $\triangle H$ = 181.06 J/g at optimal mass ratio of 85.15:14.86 (CA:OD), which is higher than the theoretically predicted latent heat of phase transition, indicating a good synergistic effect beneficial to energy storage. Solid CA exists in the form of dimer and –OH in solid OD exists in form of association, and intermolecular hydrogen bonds weakens in liquid. There are hydrogen bonds in the CA-OD binary composite PCMs, and the molecular structure changes before and after the phase transformation were similar to that of a single component CA or OD. The crystal structures of the two compounds also change and the latent heat of phase transformation is improved. Finally, through TG and high and low temperature cycle test, CA-OD binary PCMs demonstrates good thermal stability and practicability in the field of building energy conservation.

1. Introduction

The global energy consumption is increasing rapidly with the continuing prosperity of emerging countries and improvement of people's living standards [1]. Among the various forms of energy consumption, the building energy consumption accounts for a large proportion in the global energy consumption system, about 40% of the total energy, where heating and cooling are around 60%–70%, which is in an irreversible growth trend year by year [2,3]. Simultaneously, the energy consumption of buildings is directly correlated with greenhouse gas emissions. According to the International Energy Agency (IEA), the carbon dioxide emissions of the global construction industry account for 37% of the total emissions, and will continue to rise and contribute to global warming [4–7]. Therefore, it is urgent to reduce building energy consumption and carbon emissions and vigorously develop green buildings.

Phase change materials (PCMs) can absorb and release a large amount of heat energy, when the PCMs change from one to another phase due to the change in the subjected conditions [8,9]. Building walls with the incorporation of PCMs could temporarily store energy, thus reducing indoor temperature fluctuation, cooling and heating load, and reducing energy consumption [10–12]. Therefore, it has become an active research direction in the field of energy and building materials [12–14], and is considered to be an effective means to alleviate the energy crisis, improve the energy efficiency of buildings and achieve sustainable energy development [15,16]. However, the application of PCMs in the field of construction should meet the required thermo-physical, kinetic and chemical properties, as well as the standard of economic benefits, with high density, high latent heat and thermal

Nomenclature

Symbols

X_i	the mole fraction of substance i ($X_A + X_B = 1$)
R	the gas constant, 8.315 J/(mol· K)
T_m	the low temperature eutectic temperature of binary system, K.
T_i	the melting point of substance I, K.
H_i	the latent heat of phase transition of substance i during its melting, J/mol
H_m	the latent heat of phase change when the blend melts, J/mol
C_{psi}	the specific heat of solid i at constant pressure, J/(mol·K)
C_{pli}	the specific heat of liquid i at constant pressure, J/(mol·K)
$\triangle H$	the latent heat of phase transformation, J/g
T_p	the peak temperature, °C

Abbreviation

PCMs	Phase change materials
CA	Capric acid
OD	Octadecanol
PTT	Phase transition temperature
PLH	Phase latent heat
DSC	differential scanning calorimeter
XRD	X-ray powder diffractometer
ATR-FTIR	Fourier transform attenuated total reflection infrared spectroscopy
TG	thermogravimetry
DTG	derivative thermogravimetry

conductivity, stable temperature when phase change [17,18]. Organic PCMs have the advantages of good phase change reversibility and small volume change, and are not prone to supercooling and phase separation, tasteless, harmless and non-corrosive, not harmful to human body and environment, cheap and easy to obtain and separate, which has a good application prospect in the field of building energy conservation [19–22].

Nevertheless, in practice the melting temperature of a single organic PCMs is hardly able to meet the proper temperature of human body in the building envelope (22–28 °C) [23], and the phase change range is narrow, which has certain limitations in the promotion and application [24]. Therefore, the researchers used the binary combination method to obtain the composite PCMs with the required melting temperature, which has great application potential in architecture [25]. Organic composite PCMs are mainly prepared, for example, by paraffin and fatty acid [26], fatty acid and fatty acid [11,27,28], fatty acid and fatty alcohol [29–32]. Because fatty acids and fatty alcohols mainly come from the natural animal fat and vegetable oil, they have compared with paraffin lower flammability and better biodegradability [17,33]. The compounded binary composite PCM of fatty acids and fatty alcohols has good thermal stability, chemical compatibility and long-term cycling reliability, and can be a low energy consumption thermal energy storage (TES) material [34,35]. To obtain a PCMs that is more suitable for use in the built environment, the phase transition temperature (PTT) must be suitable, e.g. 22–28 °C for living environment, and the thermodynamic properties meet the requirement of the needed operations.

As a saturated decathic acid, capric acid (CA) has a low PTT, high PLH, no corrosion, good chemical and thermal stability, and is suitable for controlling the ambient temperature within the building [36,37]. Samer et al. [28] prepared a CA-MA low eutectic mixture and found it can be used to regulate temperature in passive built environments. The

CA-SA composite PCM was further vacuum impregnated into the wood [32], which effectively reduced the temperature fluctuation in the wood building and realized the energy saving of the wood building. Otadecanol (OD) is another potential component material, it belongs to the fatty alcohol class, the enthalpy of phase change is high, has good thermal stability and is inexpensive [38], while fatty acids have good compatibility with fatty alcohols. For example, fatty acids were combined with Tetradecanol to give a series of binary low-eutectic mixtures that can be used for building energy storage [32]. A binary eutectic system was also prepared from Lauric acid (LA) and Octadecanol (OD) by melting blending method [39].

The latent heat storage of PCMs mainly depends on the interaction between molecules, and the latent heat value of PCMs depends on the order of lattice structure and the strength of hydrogen bond [40]. The thermal property of organic PCMs is determined by the length of alkane chain and thermal mass transfer [41]. To improve the temperature and energy storage properties of organic PCMs, the molecular structure can be manipulated. If hydrogen bond is introduced into the PCMs derived from fatty acids, the PTT and thermal stability may be significantly improved. In this work, a simple low eutectic method was used to prepare a composite PCMs system of Capric acid (CA) and Octadecanol (OD), and the behavior of phase transformation storage and heat release was analyzed through theoretical calculation and experimental assessment. The structural changes caused by the heat absorbed and released during the phase transformation are also examined by the measurement of ATR-FTIR and XRD to further understand the phase changing and heat storage mechanisms of CA-OD binary composite PCMs, providing a theoretical basis for the screening, modification and innovation of organic composite PCMs. Finally, the thermal stability of CA-OD binary composite PCMs was tested by TG and high and low temperature cycling. This development aims to illustrate the binding principle and transformation mechanism of binary PCMs of fatty acids and fatty alcohols, so as to provide a new generation of PCMs and generate positive impact on the utilization of composite PCMs for building energy conservation.

2. Materials and methods

2.1. Materials

Capric acid (CA, $C_{10}H_{20}O_2$) for experimental use in this study was purchased from Shanghai Zhanyun Chemical Co. LTD. and Octadecanol (OD, $C_{18}H_{38}O$) purchased from Sinopsin Chemical Reagent Co. LTD. The properties of the commercial PCMs provided by the manufacturers are summarized in Table 1.

2.2. Preparation of CA-OD binary composite PCMs

2.1.1. Theoretical consideration of thermal properties of binary composite PCMs

According to the second law of thermodynamics and the theory of phase equilibrium [33,34], the best molar ratio and the minimum crystallization temperature of the binary composite PCMs can be obtained by Schroeder's formula (1).

$$\frac{1}{T_m} = \frac{1}{T_i} - \frac{RlnX_i}{H_i} \quad (I=A, B) \tag{1}$$

Where, T_m is the eutectic temperature of binary system (K), T_i is the

Table 1
Parameters of the commercial PCM materials.

Material	Purity class (ω/%)	Melting temperature/°C	Molecular weight
CA	≥99.0%	≥29.0	172.26
OD	≥99.0%	56.0–59.0	270.50

melting point of substance i (K), X_i is the mole fraction of substance i (X_A + X_B = 1), H_i is the latent heat of phase transition of substance i during its melting (J/mol), R is the gas constant, 8.315 J/(mol· K). The result obtained by equation (1) can draw a phase diagram of the binary eutectic system and determine the eutectic point.

For PCMs, there is a little difference in phase change temperature, no chemical reaction occurs during the recombination, it has nothing to do with the process, entropy is only a parameter [35], therefore, the theoretical phase transition latent calorific value of the mixture can be expressed in equation (2).

$$H_m = T_m \sum_{i=1}^{n} \left[\frac{X_i H_i}{T_i} + X_i \left(C_{pli} - C_{psi} \right) ln \frac{T_m}{T_i} \right] \qquad (2)$$

Since the latent calorific value of the phase change material is much greater than the sensible calorific value [25,33], equation (2) can be reduced to equation (3).

$$H_m = T_m \sum_{i=1}^{n} \left[\frac{X_i H_i}{T_i} \right] \qquad (3)$$

Where, T_m is the low temperature eutectic temperature of binary system (K), T_i is the melting point of substance i (K), X_i is the mole fraction of substance i (X_A + X_B = 1), H_i is the latent heat of phase transition of substance i during its melting (J/mol), R is the gas constant, 8.315 J/(mol· K), H_m is the latent heat of phase change when the blend melts (J/mol), C_{psi} and C_{pli} are the specific heat of solid and liquid i at constant pressure [J/(mol·K)], respectively.

2.1.2. Preparation of binary composite PCMs

The binary composite PCMs was synthesized by way of the mixed melting based on the theoretical calculation, and the preparation process was shown in Fig. 1. CA-OD binary eutectic systems with different mole ratios were prepared to study their thermal properties understand their functions and interactions in the mix and identify the best mass ratio of eutectic points. According to different mole ratios, a certain amount of CA and OD was weighed and placed into a 10 ml test tube, which was then sealed and heated in an electric constant temperature oscillation tank (DKZ, Shanghai Yiheng Technology Co. LTD) at 75 °C until melting to obtain a molten blend. Then, the mixture was placed in a CNC ultrasonic cleaner (KH-500DE, Kunshan Hechuang Ultrasonic Instrument Co. LTD) with a water bath temperature of 75 °C and a power of 100 W, and the mixture was treated with ultrasonic for 30min to make it mixed evenly. Finally, the mixture was taken out and cooled to room temperature to obtain CA-OD binary composite PCMs with different molar ratios.

2.2. Characterization

2.2.1. Hot melt - step cooling test

In order to understand the interaction of CA and OD, identify the best mole ratio and eutectic point of CA-OD binary composite PCMs, CA-OD mixtures with different mole ratios are tested by the hot melt-step cooling curve method, the test process is shown in Fig. 2. The test tube containing CA-OD binary composite PCMs was put into a 75 °C constant temperature water bath (DC-0506 W, Shanghai Pingxuan Scientific Instrument Co. LTD), and insert a thermocouple (K type, Accuracy: ±1 °C, Zhongxiang Instrument Co. LTD.) in the center of the test tube after the PCMs are completely melted and ensure that it does not touch the inner wall of the tube. Meantime, heat in a 75 °C of water bath for 1 h. Then, the sample was quickly placed into a 5 °C low temperature water bath until a complete crystallization is achieved. Finally, the sample was quickly placed into a 75 °C constant temperature water bath until a completely melted. Water was also tested as a reference. The thermal couple was connected to a temperature inspection instrument (DC5516U, Zhongxiang Instrument Co., LTD.) and the sample temperature was recorded continuously with an interval of 10s.

2.2.2. Sample characterization

The phase transition temperature and latent heat of CA, OD and CA-OD composite PCMs were measured by DSC (X3, TA company, Accuracy 0.01 °C) the test conditions of which are the sample mass of 5–7 mg, the temperature range of 10°C–90 °C, temperature rise and fall rate of 10 °C/min, N2 atmosphere and nitrogen flow 50 mL/min. The crystal structures of CA, OD and CA-OD binary composite PCMs were tested by XRD (D8ADVANCE, Bruker company, accuracy 0.01°). The diffraction source was copper target, the diffraction angle was 5°–60°, the voltage was 40 kV, the current was 40 mA and the scanning rate was 5°/min. The structure and composition of CA, OD and CA-OD binary composite PCMs were analyzed by ATR-FTIR (iS5, Nicolet company, accuracy 0.01 cm-1). The test conditions were as follows: 32 scanning times, measurement range of 4000–500 cm^{-1} and resolution of 4 cm^{-1}. The thermal decomposition stability of CA-OD binary composite PCMs was tested by TGA (Q5000, TA, USA, accuracy:±0.01 °C). The test conditions were heating from 25 °C to 500 °C in a N2 atmosphere at a heating rate of 10 °C/min. To explore the thermal stability of CA-OD binary composite PCMs, the prepared sample is put into a programmable high and low temperature circulation box (HKGD-100, Dongguan Huakai Testing Equipment Technology Co., LTD.), the temperature is set at 75 °C for 60min to completely melt the sample, and then the sample is completely crystallized by cooling to 10 °C at 2 °C/min for 60 min, and finally heated to 75 °C for 60 min the above experimental process was cycled for 1000 times. The DSC test was carried out when the number of
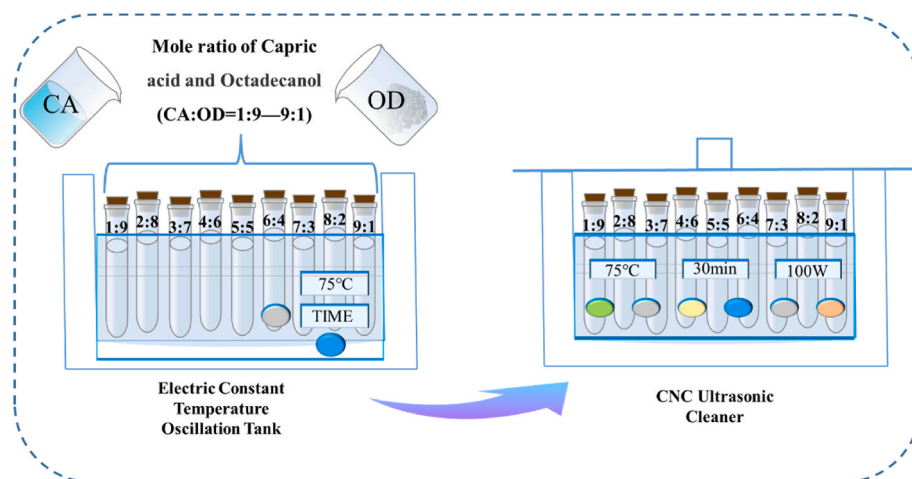

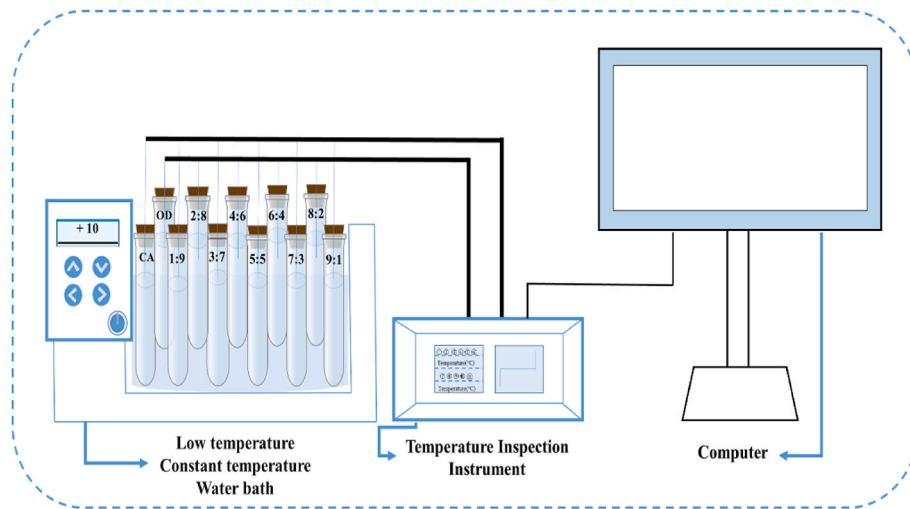**Fig. 1.** Preparation process of CA-OD binary composite PCMs.

Fig. 2. The test process of hot melt-step cooling.

cycles reached 0 and 1000 cycles.

3. Results and discussion

3.1. Theoretical prediction of phase transition temperature and latent heat of CA-OD composite

To predict the phase transition temperature and latent heat of a eutectic composite PCMs, the DSC curves of the CA and OD used in the experiment are produced (Fig. 3). It can be seen that both the phase transition temperature and latent heat are much higher for OD than for CA PCMs. The phase transition temperature of CA is 30.23 °C and the latent heat of the phase change is 169.17 J/g. The transition temperature of OD is 55.86 °C and the latent heat of the phase change is 249.15 J/g. The other calculated parameters are also given in Table 2.

The related calculation parameters in Table 2 were substituted into Eq (1) to calculate the solid-liquid diagram of CA-OD binary composite PCMs, as shown in Fig. 4.

$$\frac{1}{T_m} = \frac{1}{303.63} - \frac{8.315 \ln X_{CA}}{29141.22} \tag{4}$$

$$\frac{1}{T_m} = \frac{1}{329.01} - \frac{8.315 \ln X_{OD}}{67391.23} \tag{5}$$

Table 2
Related calculation parameters for CA and OD.

Component	Phase melting point		Latent heat of fusion	
	T_m (°C)	T_m(K)	H (J/g)	H (J/mol)
CA	30.48	303.63	169.17	29141.22
OD	55.86	329.01	249.15	67391.23

$$X_{CA} + X_{OD} = 1 \tag{6}$$

$$\frac{M_{CA}}{M_{OD}} = \frac{X_{CA} \times 172.26}{X_{OD} \times 270.49} \tag{7}$$

$$M_{CA} + M_{OD} = 1 \tag{8}$$

Fig. 4 shows that the theoretical molar ratio of CA-OD binary composite PCMs is 90:10, and the mass ratio is $M_{CA}:M_{OD} = 85.15:14.86$ converted by (7) and (8). In addition, the theoretical melting temperature of the CA-OD binary composite PCMs is calculated as 300.88 K (27.73 °C).

Finally, substitute the calculated molar ratio and the theoretical melting temperature into Eq. (3) to obtain the latent heat of CA-OD is 176.65 J/g.
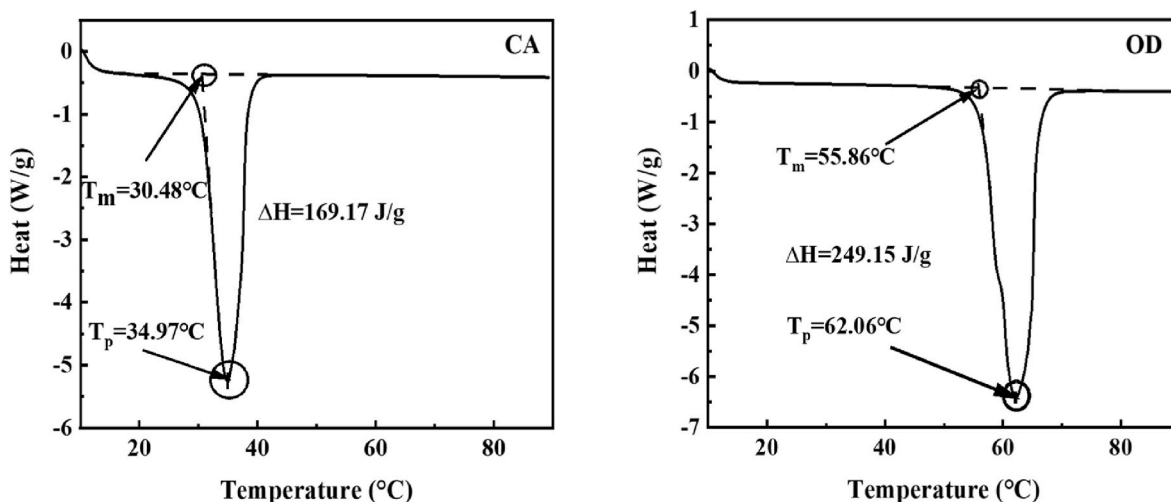

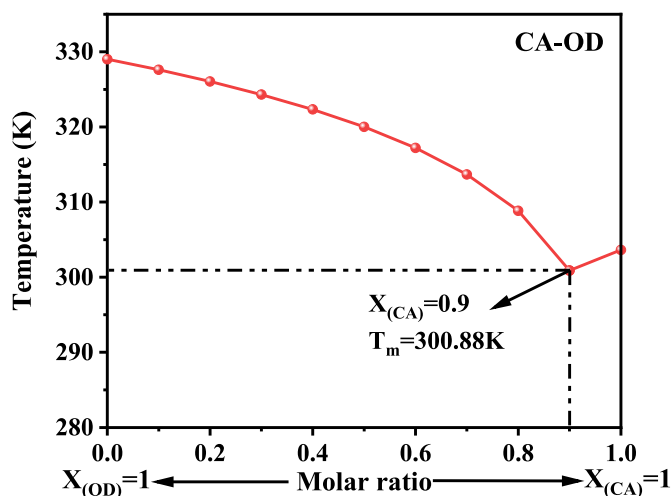**Fig. 3.** DSC hot melt curves of CA and OD.

Fig. 4. T-X phase diagram of CA-OD binary composite PCMs.

$$H_m = 300.88 \times \left(\frac{0.9 \times 29141.22}{303.63} + \frac{0.1 \times 67391.23}{329.01} \right) \quad (9)$$

3.2. Hot melt-step cooling curves analysis of CA-OD binary composite PCMs

The hot melting and step cooling curves of CA-OD binary composite PCMs at different mole ratios (CA:OD = 1:9–9:1) are shown in Fig. 5a and b. Phase transformation in binary composite PCMs occurs at different time and different temperature depending on molar ratios. The hot melting and crystallization temperatures of binary composite PCMs gradually decrease with the increase of CA mole fraction (Fig. 5 inset). It seems from Fig. 3a that in the hot melting process, there are three different behavior of phase transitions: when the molar ratio of CA-OD is 1:9 and 2:8, binary composite PCMs undergoes single phase transition at around 500s with the PTT is 51.16 °C and 50.70 °C, respectively; With the increase of the molar fraction of CA, in the range of 0.3–0.7, the mixed system undergoes two step phase transition with the first transition occurring at around 200s and 20 °C and the second around 500s and 45 °C. When the molar fractions of CA are 0.8 and 0.9, there is single phase transition in the mixed system, and the phase transition takes place at 200s with temperatures being 23.00 °C and 22.90 °C, respectively. In the cooling crystallization process (Fig. 5b), the corresponding eutectic temperatures of the CA-OD binary eutectic system are 54.50 °C and 52.20 °C at 1:9 and 2:8, respectively; similar to those at heating process there is a secondary phase transition occurred when the molar ratios are 3:7, 4:6, 5:5, 6:4 and 7:3. When the molar fraction of CA is 0.8 and 0.9, the crystallization temperature is 27.2 °C and 26.5 °C, respectively. In summary, when the molar fraction of CA is around 0.9, both the melting point and the crystallization point are lowest. This shows that CA and OD are physicochemical mixtures, when their molar ratio is in the range of (1:9)-(2:8), the mixed system is dominated by OD, which can be due to the formation of intermolecular forces between all CA molecules and some OD molecules, resulting in the PTT of the mixing system slightly lower than pure substance OD. With the gradual increase of CA content, the change of the binding mode between CA and OD molecules may lead to the occurrence of secondary phase transition. When its molar ratio is in the range of (8:2)~(9:1), CA is the main body in the mixed system, which can be due to the formation of intermolecular forces between all OD molecules and some CA molecules, resulting in the PTT of the mixing system slightly lower than the PTT of pure substance CA.

In order to achieve more accurate composition of binary composite PCMs, further hot melt and step-cooling test were carried out on CA-OD binary PCMs with CA molar fractions ranging from 0.89 to 0.92 (Fig. 6).
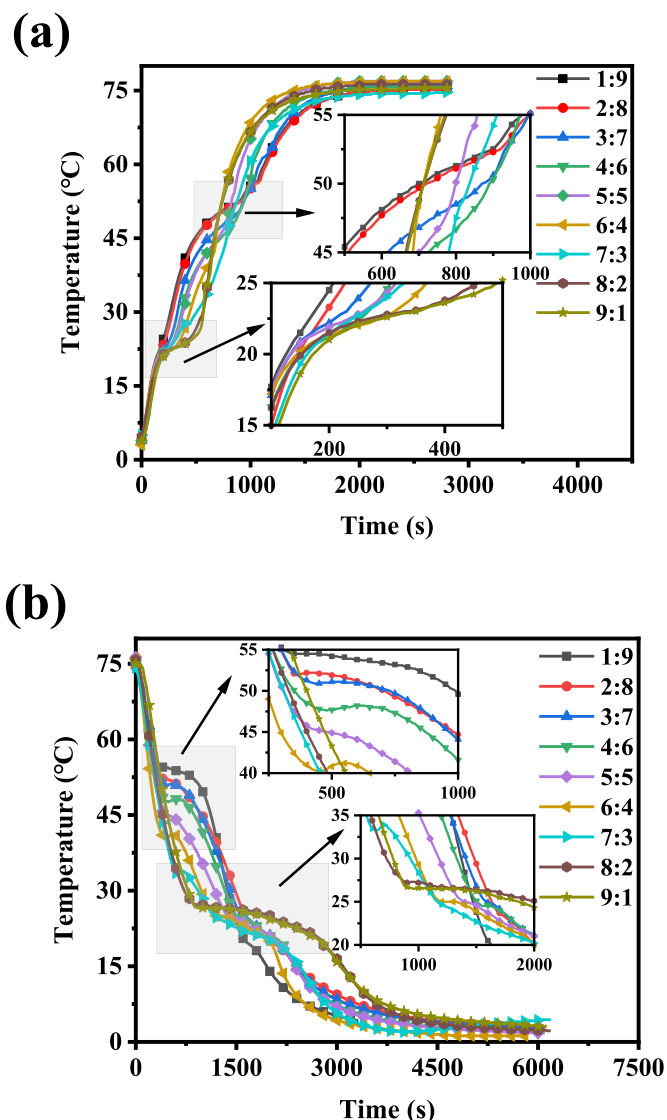

Fig. 5. (a) Hot-melt curve of CA-OD with different molar ratio; (b) step-cooling curve of CA-OD with different molar ratio.

It can be seen that with the increase of the molar fraction of CA, the hot-melt and crystallization temperature of binary composite PCMs decreases first and then increases; when the molar fraction of CA is 0.89, 0.90, 0.91 and 0.92, the hot-melt temperature is 23.00 °C, 22.90 °C, 27.10 °C and 28.30 °C, respectively, and the crystallization temperature is 27.98 °C, 26.50 °C, 28.89 °C and 28.56 °C, respectively. It is interesting that the molar fraction seems to has a significant effect on the hot-melt and crystallization process, with the increase of the molar fraction of CA, the hot-melt and crystallization point of the binary system decreases first and then increases, and the PTT of the CA-OD binary system reaches the lowest level, when the molar fraction of CA is 0.9, and there is no stratification. At the same time, it can be seen from Fig. 6b that CA and OD pure substances do not have super cooling degrees in the phase transition process, and as the ratio of CA-OD binary systems tends to be low eutectic molar ratio, its super-cooling degree gradually becomes smaller, and when the optimal molar ratio is reached 9:1, there is no obvious super-cooling degree, indicating that the nucleation ability of CA-OD binary composite PCMs is better.

Therefore, it can be determined that the optimal molar ratio of CA-OD binary composite PCMs is 9:1 and its PTT is 26.50 °C, which indicates that CA-OD has pure phase property and is a low eutectic mixture.
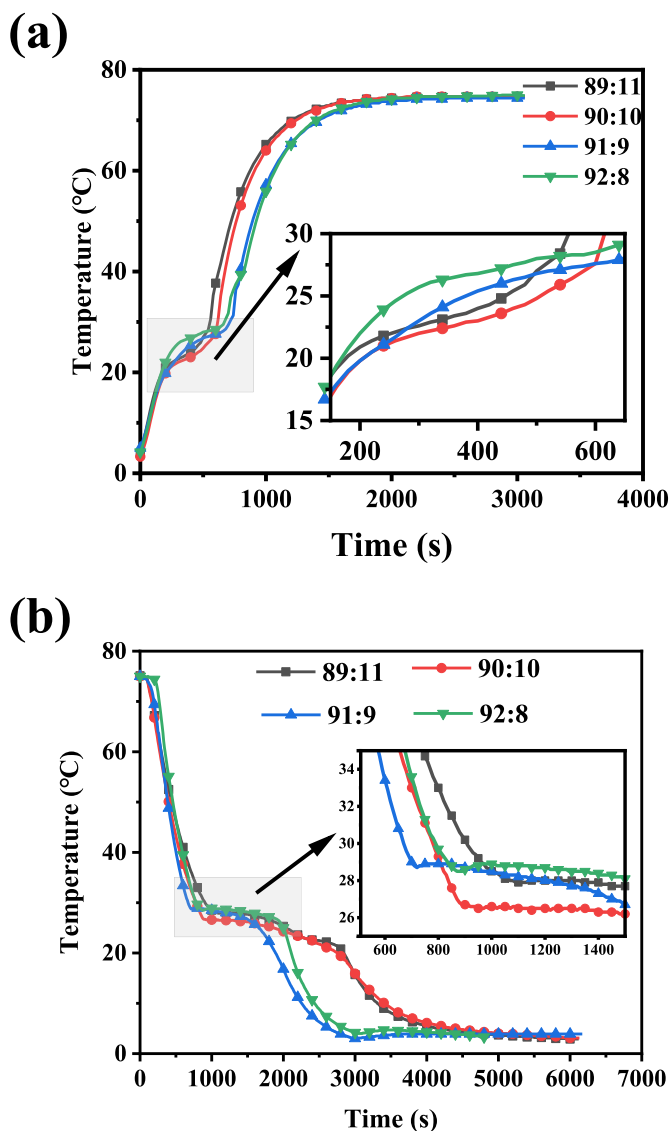
(a)

(a)

(b)

(b)

Fig. 6. (a) CA-OD binary eutectic system near hot melt point; (b)CA-OD binary eutectic system near crystalline point.

Fig. 7. (a) Hot melt curve of CA, OD and CA-OD; (b) step cooling curve of CA, OD and CA-OD.

The hot-melting and step-cooling curves of CA, OD and CA-OD binary eutectic system are further coplotted in Fig. 7 (a, b). Among them, water sample are included as a reference. It can be seen from Fig. 7a that both CA, OD and CA-OD exhibit hot-melting and crystalline phenomenon during the heating and solidification process but with very different magnitude. The melting of CA starts from 28.33 °C and end of the 30.60 °C, duration is about 225s; OD melting temperature is 54.21 °C at the beginning and 58.61 °C at the end, duration is approximate 680s. During the cooling crystallization process, CA lasted for 1364s from 30.64 °C to 30.70 °C, and OD lasted for 359s in the temperature of 57.20 °C. That is, the hot melting rate of CA is higher than that of OD, and CA is slower than the cooling rate of OD, indicating that CA had strong exothermic capacity in heat absorption and OD is the opposite. The hot melting temperature of CA-OD binary composite PCMs starts from 21.75 °C to 25.03 °C, and the crystallization temperature during the solidification process starts from 26.48 °C to 26.50 °C. Hot melt and crystallization durations are 327s and 1035s, respectively. The melting and solidifying temperature, and the rate of heat storage and discharge of CA-OD composite PCMs have radically changed, indicating that the combination of CA and OD has changed the binding mode between molecules.
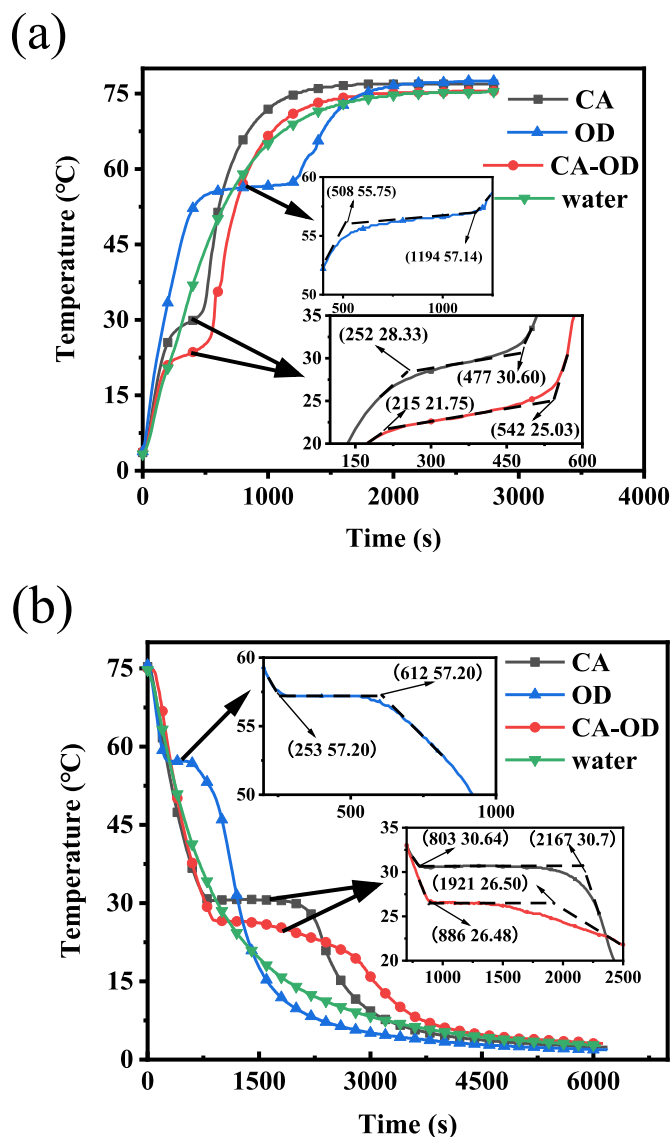
3.3. Thermal properties of CA-OD binary composite PCMs

The thermal properties of phase change materials mainly include phase transition temperature (PTT) and phase latent heat (PLH). The most common used method for obtaining both the PLH and PTT of PCMs is the DSC test to obtain the curve diagram of temperature and heat flow value. Natural convection could accelerate the heat transfer between the phase front and the heat transfer fluid in PCMs energy storage systems and this phenomenon will also affect the DSC test results of PCMs [42–44]. Therefore, in the process of DSC testing, in order to limit the influence of natural convection when the PCM samples are the liquid phase [42,43,45], it is necessary to select appropriate test conditions, such as a small amount of samples (generally in the range of 5–10 mg), low heating rate (such as 10 °C/min or 5 °C/min) and small crucibles (about 10 μl) for measurement [46,47], and this is followed in the study. In summary, according to the DSC test conditions (2.2.2) of CA-OD binary composite PCMs, the influence of natural convection on its thermal properties is considered very limited compared to the overall tested results and such can be ignored.

The thermal performance of CA-OD binary composite PCMs with different molar ratios are investigated by DSC (Fig. 8). As can be seen
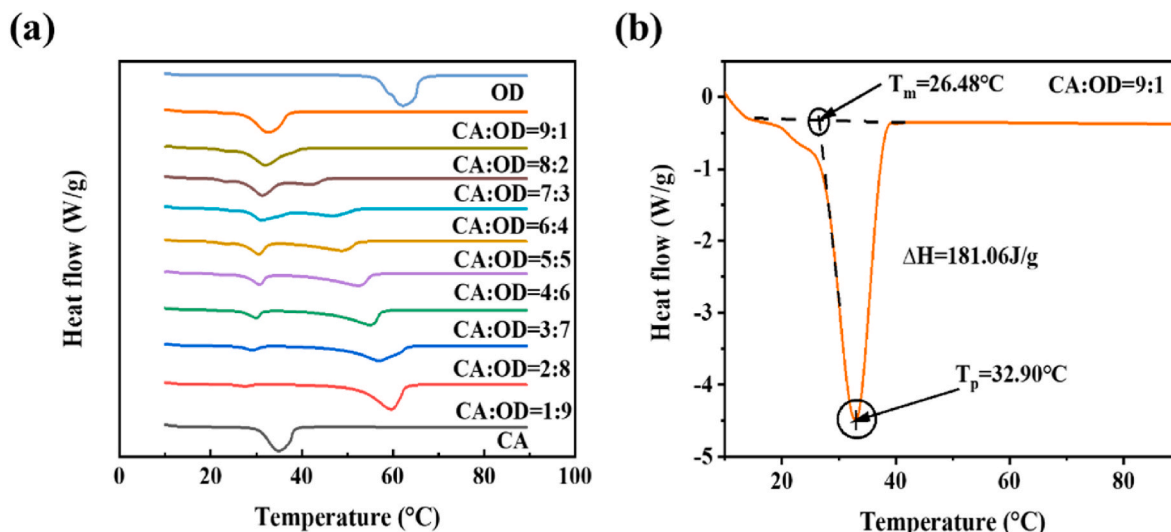
Fig. 8. (a) DSC curves of CA-OD binary eutectic system with different molar ratios; (b) DSC curves of CA-OD = 9:1.

from Fig. 8a, when the molar fraction of CA increases from 0.1 to 0.2 in the CA-OD mixture system, the heat flow has a single absorption peak, which shifts from high temperature to low temperature. With the gradual increase of the molar fraction of CA, in the range of 0.3–0.7, there is a double absorption peak of heat flow. The width between the double absorption peaks gradually narrows and shifts to low temperature. When the molar fraction of CA increases to 0.8 and 0.9, the heat flow absorption peak changes from bimodal to single peak and the temperature is slightly lower than CA. When CA:OD = 9:1 (Fig. 8b), only one endothermic peak appears in the binary eutectic heat curve and no splitting peak appears, which is very similar to the DSC curve of pure material, indicating that CA and OD eutectic is good. The initial temperature of CA-OD binary eutectic is 26.48 °C, the peak temperature is 32.90 °C and the PLH is181.06 J/g. A scrutiny of the initial and peak temperatures for CA-OD binary system and pure CA and OD indicates that CA and OD are more than simply physical combinations. Comparing the theoretical calculation of CA-OD binary systems with the enthalpy results of phase change tests in DSC could show that the combination of the two had a physicochemical effect.

3.4. Structure and mechanism analysis of CA-OD binary composite PCMs

3.4.1. ATR-FTIR of CA and OD

Fig. 9 shows the ATR-FTIR spectra of CA and OD at 4000 cm^{-1}-500cm^{-1} before and after the phase transformation. As can be seen from the Figure, there are six main functional groups of CA before phase transition, including $\nu_{as-CH2-}$, ν_{s-CH2-}, $\nu_{C=O}$, ν_{C-OH}, $\delta_{C-O-H\ in-plane}$ and $\delta_{C-O-H\ on-plane}$. The characteristic absorption peaks corresponding to these functional groups are located at 2920 cm^{-1}, 2850 cm^{-1}, 1690 cm^{-1}, 1290 cm^{-1}, 1430 cm^{-1} and 930 cm^{-1}, respectively [48,49]. In addition, three δ_{C-H} peaks from CH$_2$ on CA chain are observed at 1200-1280 cm^{-1}. The main functional groups for OD before phase transformation are ν_{O-H}, $\nu_{as-CH2-}$, ν_{s-CH2-}, δ_{C-O-H}, $\delta_{C-O-H\ in-plane}$ and $\nu_{C-OH\ out-plane}$, and the corresponding characteristic absorption peaks are located at 3320 cm^{-1}, 2910 cm^{-1}, 2850 cm^{-1}, 1060 cm^{-1}, 1460 cm^{-1} and 719 cm^{-1} respectively [50].

Both the position and intensity of the characteristic absorption peaks of the functional group of CA and OD changed after the phase transition (Table 3). It can be seen that the main functional groups of CA, namely $\nu_{C=O}$, $\nu_{as-CH2-}$, ν_{s-CH2-} and δ_{C-O-H}, have shifted to a higher wave number, while ν_{C-OH} and δ_{C-O-H} have shifted to a lower wave number. This may be due to that the fatty acids mainly exist in the form of dimer connected by hydrogen bond (C=O···H–O) and the strength of hydrogen bond bonding usually causes the reverse change of stretching vibration

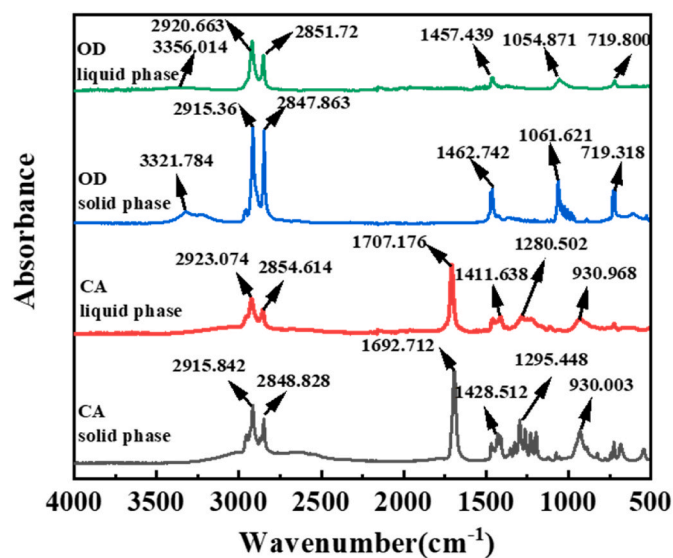**Fig. 9.** ATR-FTIR before and after CA and OD phase transition.

frequency of C=O [51]. On the other hand, the vibration frequency of C–OH bond is proportional to the induction effect of the electron absorbing group C=O [52], so the blue shift of $\nu_{C=O}$ after phase transformation indicates that the hydrogen bond strength of CA dimer decreases and the red shift of C–OH bond after phase transformation further confirms that the hydrogen bond strength decreases. Meanwhile, due to the positive effect of steric hindrance on the frequency of deformation vibration, the red shift of δ_{C-O-H} and the weak blue shift of δ_{C-O-H} indicate that the hydrogen bond of CA dimer has a greater effect on the vibration of C–O–H [53]. It is also observed in Table 3 that the absorption intensity of the main functional groups of CA after phase transformation decreases in different amplitude, among which the absorption intensity of ν_{C-OH} and ν_{as-CH2} decreases the most, by 0.154 and 0.140 respectively. In addition, no characteristic absorption peak of δ_{C-H} is observed. The results indicate that the intermolecular hydrogen bond bonding ability of CA is weakened after the phase transition, and the CA main carbon chain changes from highly ordered all-trans conformation to disordered conformation.

The ATR-FTIR changes of OD at different temperature indicate that after the phase transformation, the main OD functional groups, ν_{O-H}, ν_{as-}

Table 3
Changes of FTIR absorption peaks corresponding to characteristic functional groups before and after CA and OD phase transition.

	Bonds	Wavenumber(σ/cm^{-1})			Absorbance		
		Solid phase	Liquid phase	$\Delta(\sigma)$	Solid phase	Liquid phase	$\Delta(A)$
CA	$\nu_{as\text{-}CH2\text{-}}$	2915.842	2923.074	7.232	0.367	0.227	−0.140
	$\nu_{s\text{-}CH2\text{-}}$	2848.828	2854.614	5.786	0.274	0.155	−0.119
	$\nu_{C=O}$	1692.712	1707.176	14.464	0.591	0.453	−0.137
	$\nu_{C\text{-}OH}$	1295.448	1280.502	14.946	0.268	0.114	−0.154
	$\delta_{C\text{-}O\text{-}H \text{ in-plane}}$	1428.512	1411.638	16.874	0.174	0.110	−0.064
	$\delta_{C\text{-}O\text{-}H \text{ out-plane}}$	930.0032	930.9675	0.964	0.195	0.094	−0.101
OD	$\nu_{O\text{-}H}$	3321.784	3356.014	34.23	0.066	0.022	−0.044
	$\nu_{as\text{-}CH2\text{-}}$	2915.36	2920.663	5.303	0.636	0.332	−0.304
	$\nu_{s\text{-}CH2\text{-}}$	2847.863	2851.72	3.857	0.610	0.234	−0.376
	$\nu_{C\text{-}OH}$	1061.621	1054.871	−6.75	0.282	0.077	−0.205
	$\delta_{C\text{-}O\text{-}H \text{ in-plane}}$	1462.742	1457.439	−5.303	0.221	0.088	−0.133
	$\delta_{C\text{-}O\text{-}H \text{ out-plane}}$	719.318	719.800	0.482	0.217	0.0651	−0.152

$_{CH2\text{-}}$, $\nu_{s\text{-}CH2\text{-}}$ and $\delta_{C\text{-}O\text{-}H}$ have shifted to a higher wave number, while $\nu_{C\text{-}OH}$ and $\delta_{C\text{-}O\text{-}H}$ have shifted to a lower wave number. Because of $\nu_{O\text{-}H}$ free hydroxyl ($\nu_{O\text{-}H}$) absorption peak in the range of 3600–3650 cm^{-1}, associating hydroxyl ($\nu_{O\text{-}H}$) absorption peak in the range of 3100–3600 cm^{-1} [37]. Therefore, when OD is solid state, it can be seen that only the associated hydroxyl absorption peak (3321.784cm-1) has no free hydroxyl absorption peak in ATR-FTIR. This indicates that when OD is in solid state, the strength of O–H bond increases due to the formation of intermolecular hydrogen bond, and the absorption peak moves to low frequency, that is, OD exists in the form of –OH association. Meanwhile, the out-of-plane deformation vibration peak of C–O–H is generally located in the range of 800–225 cm^{-1}, if the –OH association absorption peak occurs, it moves to the range of 750–650 cm^{-1}, and the $\delta_{C\text{-}O\text{-}H \text{ out plane}}$ is located at 719.318 cm^{-1}, which further indicates there are association state of OH in solid OD. With the increase of temperature, OD from solid phase to liquid phase, the $\nu_{O\text{-}H}$ wave number blue shift to 3356.014 cm^{-1}, this is mainly caused by to the O–H bond becomes stronger, O–H bond length becomes shorter, resulting in the OD molecular hydrogen bond strength weakened [54]. Meanwhile, the red shift of $\nu_{C\text{-}OH}$ and $\delta_{C\text{-}O\text{-}H \text{ in plane}}$ also indicates that the hydrogen bond strength between OD molecules is weakened. It can be seen from Table 3 that after the phase transformation the absorption peak intensity of OD functional group has different degrees of weakening. Among them, $\nu_{as\text{-}CH2\text{-}}$ and $\nu_{s\text{-}CH2\text{-}}$ absorption peak intensity weakened most, $\nu_{as\text{-}CH2\text{-}}$ absorption peak intensity weakened 0.304, $\nu_{s\text{-}CH2\text{-}}$ absorption peak intensity weakened 0.376. And $\nu_{as\text{-}CH2\text{-}}$ and $\nu_{s\text{-}CH2}$ also appear blue shift, which indicates that OD transformation into liquid, the order of the main carbon chain is also reduced.

3.4.2. ATR-FTIR of CA-OD binary composite PCMs

The infrared spectra of CA-OD binary composite PCMs before and after phase transformation contain all characteristic peaks of CA and OD (Fig. 10, Fig. 11), and no new characteristic peaks appear, indicating that no chemical reaction occurs in the combination of CA and OD. However, the absorption peak of $\nu_{O\text{-}H}$ moved to high frequency 3675.176 cm^{-1} and almost no shift occurred after the phase transition, this may be attributed to that CA and OD are bonded by hydrogen bond in a free form.

Nevertheless, after phase transformation, the position and intensity of characteristic absorption peaks of some functional groups of CA-OD binary composites change and the specific data are show in Table 4. It is apparent that the blue shift functional groups of CA-OD binary PCMs include $\nu_{as\text{-}CH2\text{-}}$, $\nu_{C=O}$, $\delta_{C\text{-}O\text{-}Hout\text{ -plane}}$ (CA) and $\delta_{C\text{-}O\text{-}H \text{ out-plane}}$ (OD), while the functional groups with obvious red shift are $\nu_{C\text{-}OH}$ (CA), $\nu_{C\text{-}OH}$ (OD), $\delta_{C\text{-}O\text{-}H \text{ in plane}}$ (OD), and the absorption intensity of characteristic absorption peaks of $\nu_{C\text{-}OH}$ (CA), $\delta_{C\text{-}O\text{-}H \text{ in plane}}$ (OD), $\delta_{C\text{-}O\text{-}H \text{ out-plane}}$ (CA) and $\delta_{C\text{-}O\text{-}H \text{ out-plane}}$ (OD) decreases obviously probably due to the breaking of intermolecular hydrogen bonds.

A comparison between Tables 4 and 3 shows that the intensity of characteristic absorption peaks of CA-OD is lower than that of CA and OD before the combination, indicating that van der Waals force exists in their combination. In order to further verify the binding mode of CA-OD and infer its phase transformation mechanism, the absorption peak at 2910 cm^{-1} is taken as the correction band to conduct spectral subtraction between CA-OD and OD, and the obtained spectral subtraction is compared with the pure CA spectral, as shown in Fig. 9. It can be seen that the absorption peaks at 1060 cm^{-1} and 1050 cm^{-1} in the
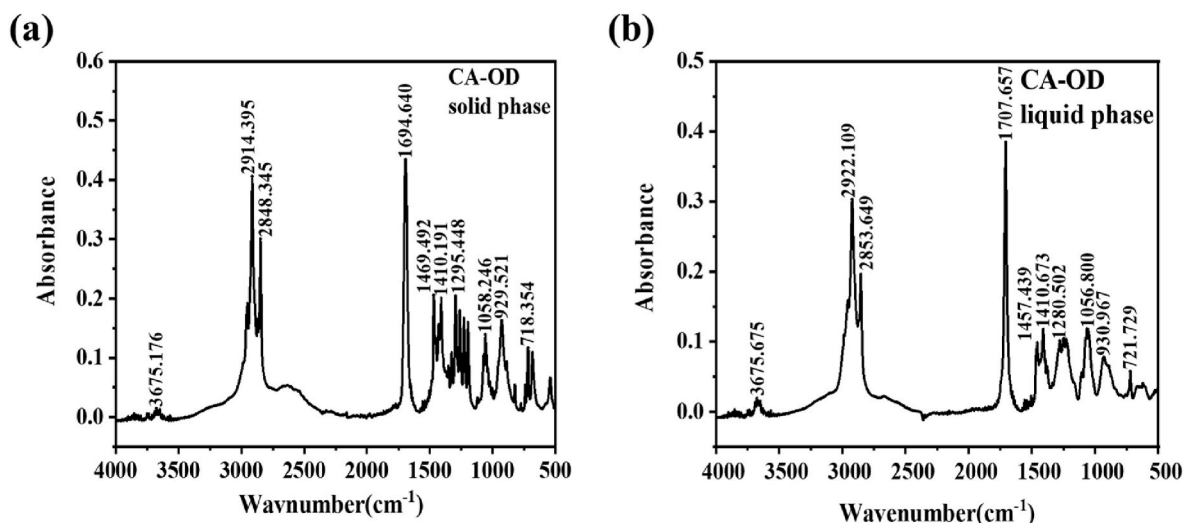

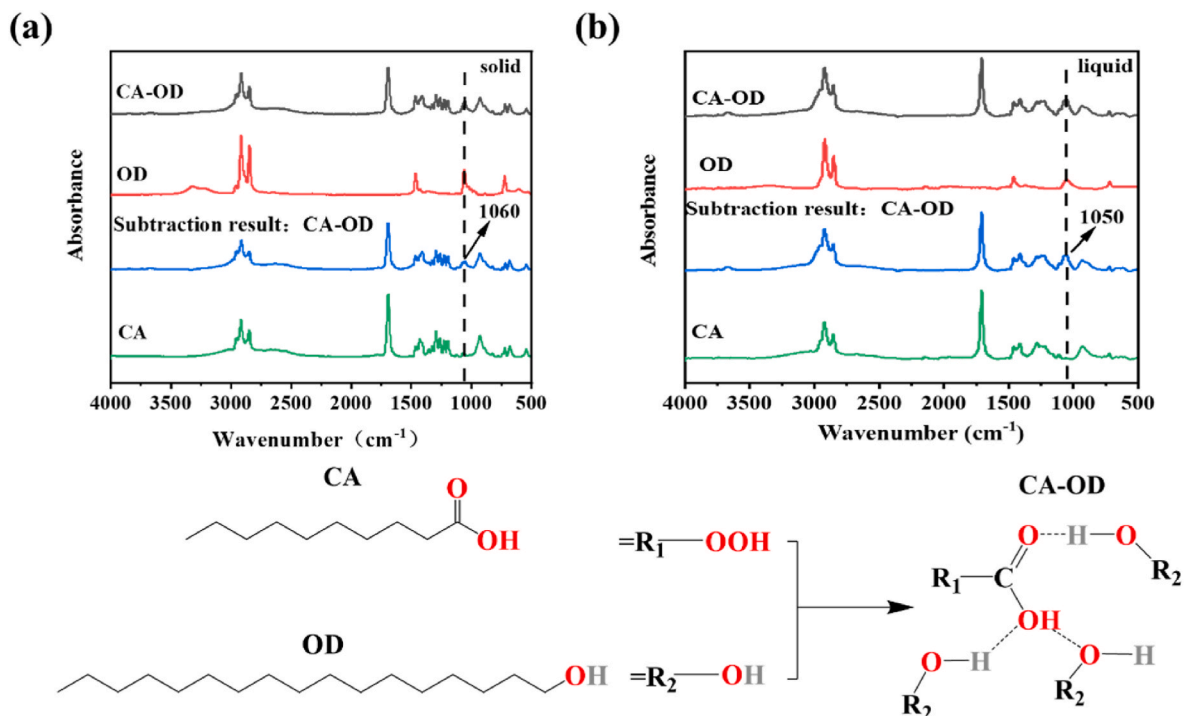**Fig. 10.** ATR-FTIR before and after CA-OD phase transition.

Fig. 11. Spectral plot of the difference before and after the CA-OD phase transition.

Table 4
Changes of ATR-FTIR absorption peaks corresponding to characteristic functional groups before and after CA-OD phase transition.

Bonds	Wavenumber σ/cm^{-1})			Absorbance (A)		
	Solid phase	Liquid phase	Δ(σ)	Solid phase	Liquid phase	Δ(A)
ν_{O-H}	3675.176	3675.657	0.481	0.0148	0.0198	0.005
$\nu_{as-CH2-}$	2914.395	2922.109	7.714	0.406	0.303	−0.103
ν_{s-CH2-}	2848.345	2853.694	5.349	0.301	0.196	−0.105
$\nu_{C=O}$	1694.64	1707.657	13.017	0.434	0.384	−0.049
ν_{C-OH} (CA)	1295.448	1280 .502	−14.946	0.204	0.101	−0.103
ν_{C-OH} (OD)	1058.246	1056.8	−1.446	0.139	0.118	−0.021
$\delta_{C-O-H\ in-plane}$ (OD)	1469.492	1457.439	−12.053	0.206	0.098	−0.108
$\delta_{C-O-H\ in-plane}$ (CA)	1410.191	1410.673	0.482	0.202	0.118	−0.084
$\delta_{C-O-H\ out-plane}$ (CA)	929.521	930.967	1.4553	0.163	0.078	−0.085
$\delta_{C-O-H\ out-plane}$ (OD)	718.354	721.729	3.375	0.117	0.057	−0.063

Fig. 12. XRD curves of CA, OD and CA-OD.

subtraction spectra before and after the phase transformation still exist, because the vibration of ν_{C-OH} and δ_{C-O-H} in hydroxyl group is very sensitive to hydrogen bond [55], forming strong hydrogen bond with carboxyl group, which may be the main reason why the latent heat of CA-OD phase transformation is lower than CA and OD.

3.5. Crystal structure of CA-OD binary composite PCMs

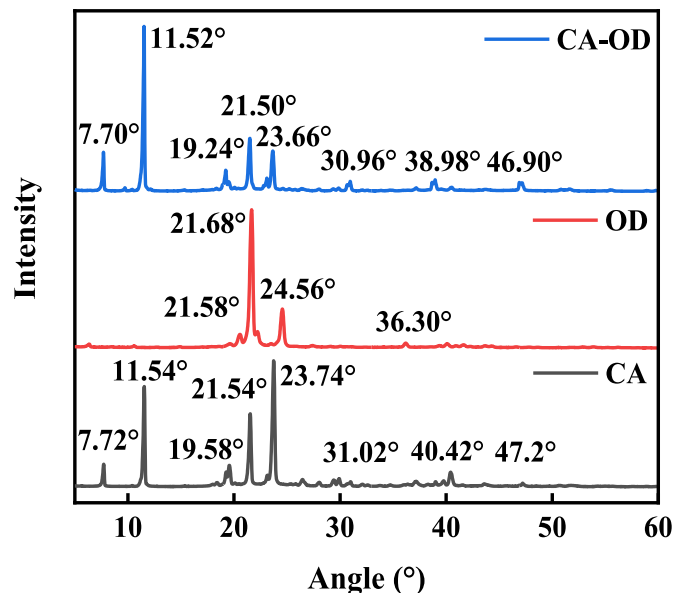The XRD test results for CA, OD, and CA-OD binary composite PCM are shown in Fig. 12. It is clear from the XRD plot of CA that diffraction peaks appear at 7.72°, 11.54°, 19.58°, 21.54°, 23.74°, 29.94°, 40.42° and 47.2°; the four diffraction peaks of the OD are located at 20.58°, 21.68°, 24,56° and 36.3°, respectively. In the XRD of CA-OD, it can be seen that the low-eutectic system contains the diffraction peaks of CA and OD, and no new diffraction peaks appear, indicating that no chemical reaction occurs between the two. At the same time, comparing the pure sample CA and OD, it is found that the diffraction peak strength at 7.70°, 11.52° and 46.9° became stronger, while the diffraction peak strength at 19.24°, 21.50°, 23.66°, 30.96° and 38.98° weakened, and shifted to the low angle direction. This can be explained that the binary eutectic system obtained after the introduction of OD mixing in CA changes the crystal structure of each other [56]. The partial diffraction

peak is significantly shifted to the left, indicating that the lattice constant becomes larger, most likely caused by the presence of macroscopic residual stress in the CA-OD eutectic system [57].

3.6. Thermal reliability of CA-OD binary composite PCMs

The thermal cycle stability and thermal decomposition stability of CA-OD binary composite PCMs are shown in Fig. 13 (a, b and c), after 1000 cycles (Fig. 13b), and the mass loss of the sample at typical temperature are listed in Table 5. The experimental results show that T_m/T_p decreases from 26.48 °C/32.90 °C–26.36 °C/32.38 °C after thermal cycle test of CA-OD binary composite PCMs; The PLH ($\triangle$H) decreased by 4.72% from 181.06 J/g to 172.51 J/g. In addition, CA-OD binary composite PCMs begins to decompose at 100 °C, the decomposition rate reaches the maximum when the temperature is 215 °C, and the sample is basically completely decomposed when the temperature rises to 331 °C. In summary, CA-OD binary composite PCMs has good thermal stability and meets the requirements of building materials.

Table 6 summarizes the reported thermal performance of bio-based binary composite PCMs. Compared with other bio-based binary PCMs, CA-OD binary composite PCMs have suitable PTT, higher latent heat of phase change and better thermal stability, which has a wide range of application prospects in the field of building energy conservation.

4. Conclusions

A new CA-OD binary composite PCMs is successfully prepared by simple melt blending method for use in building thermal energy storage systems. The lowest confluence point of CA-OD binary composite PCMs

Table 5
Mass loss rates of sample at typical temperatures.

Sample	Temperature(°C)	Mass loss rate (%)
CA-OD	100	99.99
	150	97.90
	215	47.45
	294	5.46
	331	0.16

is at a molar ratio of 9:1, giving rise to the transition temperature and latent heat of predicted 27.73 °C and 176.65 J/g, and experimentally tested 26.48 °C and 181.06 J/g, respectively. The hot melt-step cold curve storage and exothermic rate of CA-OD binary composite PCMs changed compared to the single component PCM, and the initial temperature and peak temperature are offset to low temperature, which indicated an intermolecular force in the binding mode of CA and OD. CA existed in the form of dimer in solid state and the dimer structure changed when it is liquid. The ordered molecular chains became disordered and the intermolecular hydrogen bond is weakened. The position and intensity of the characteristic absorption peak of OD changed, indicating that OD mainly existed as –OH association when it is solid, and the intermolecular is bound by hydrogen bonds. After the phase transition, the hydrogen bonding strength between the OD is reduced when it is liquid, and the order of the main carbon chain is reduced. The characteristic absorption peaks of CA and OD existed on ATR-FTIR curves of CA-OD binary composite PCMs, indicating that CA and OD acted together through molecular forces without chemical reaction. Differential analysis confirmed a hydrogen bond in the
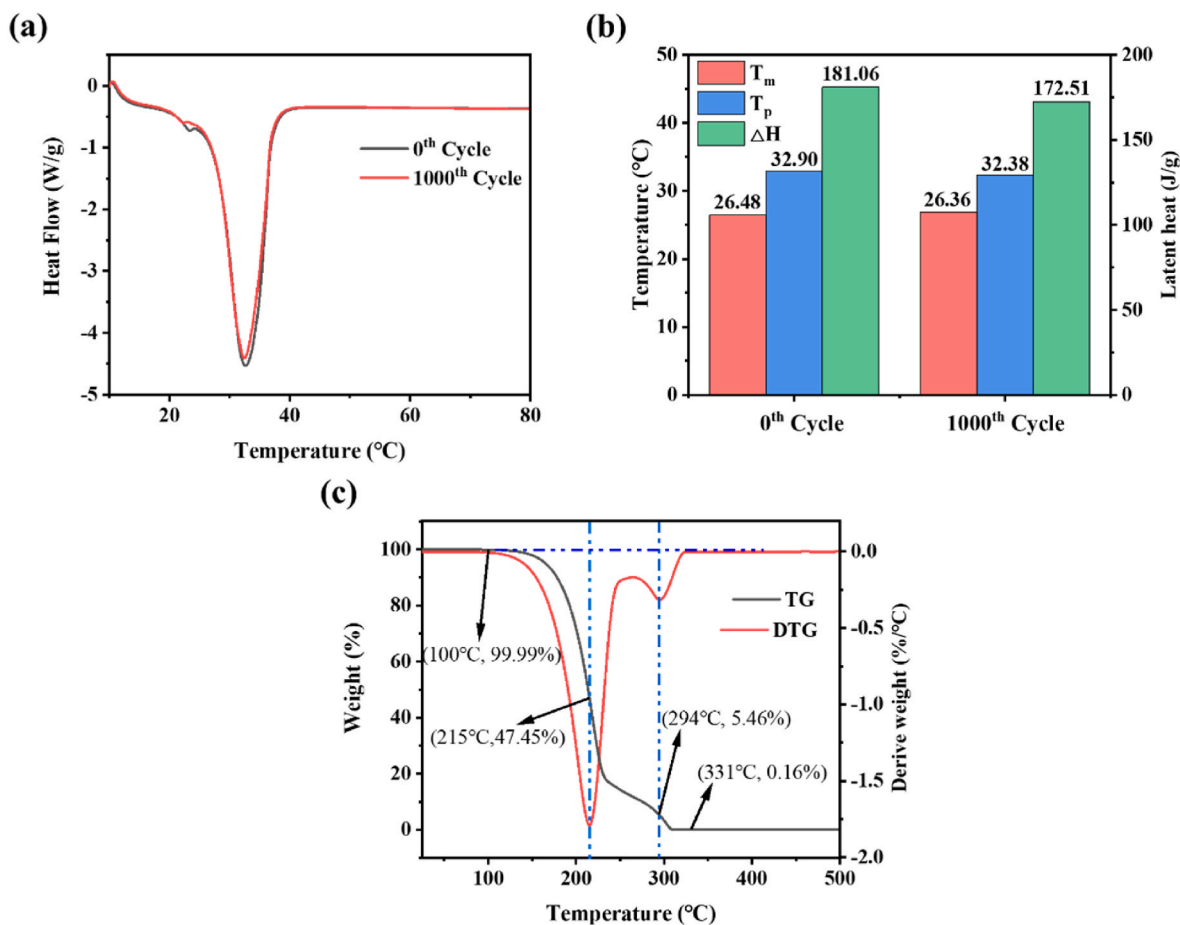
Fig. 13. The thermal cycle stability and thermal decomposition stability of CA-OD binary composite PCMs: (a) DSC curves of before and after 1000 thermal cyclic test, (b) PTT and PLH of before and after cycle and (c) TG and DTG.

Table 6
Thermal properties of reported binary composite PCMs.

PCMs	Melting temperature (°C)		Melting enthalpy (J/g)		Thermal decomposition temperature (°C)		Reference
	Before cycle	After cycle	Before cycle	After cycle	Initial	Complete	
OM-21:Dodecanol	2.09	3.11 (30th)	140.64	139.66 (30th)	101.06	218.02	[29]
1-Dodecanol: Lauric acid	17	–	175.3	–	–	–	[31]
1-Dodecanol: Myristic acid	18.43	–	180.8	–	–	–	
1-Dodecanol: Palmitic acid	20.08	–	191	–	–	–	
Myristic acid: Paraffin wax	41.89	41.35 (500th)	171.42	172.77 (500th)	137.86	297.62	[58]
Stearic acid: Myristic acid	49.83	45.41	187.54	178.12	197.69	281.81	[59]
Lauric acid: Myristic acid	35.10	34.66 (500th)	166.18	157.36 (500th)	126.51	258.13	[60]
Lauric acid: Palmitic acid	37.15	36.34 (500th)	183.07	167.41 (500th)	135.70	252.59	
Lauric acid: Stearic acid	39.29	38.54 (500th)	189.50	175.85 (500th)	110.08	276.25	
Lauryl alcohol: Cetyl alcohol	20.01	21.44 (1000th)	191.63	163.36 (1000th)	169.69	–	[61]
Capric acid: Octadecanol	26.48	26.36 (1000th)	181.06	172.51 (1000th)	100	331	This study

composite of CA and OD formed between –OH group from OD and carbonyl group from CA or between –OH group from OD and –OH group from CA. XRD analyzed structure and morphology of CA-OD binary composite PCMs indicated no new material produced after CA and OD melting blending, and the crystallinity is obviously lower than that of single CA and OD, which indicated that the crystal structure after compounding has changed. Moreover, CA-OD binary PCMs exhibited excellent thermal decomposition stability and thermal cycle stability below 100 °C and after 1000 cycles.

In the study of the mechanism of phase transformation, only the chemical structure changes before and after phase transformation were analyzed, and the systematic study and analysis of the phase transformation process require more work, which features future research direction.

Credit author statement

Peixian Zuo: Investigation, Methodology, Conceptualization, Writing. Zhong Liu: Investigation, Formal analysis. Hua Zhang: Investigation, Formal analysis. Dasong Dai: Supervision, Project administration, Funding acquisition, Review & editing. Ziyan Fu: Conceptualization, Analysis. Jorge Corker: Conceptualization, Review. Mizi Fan: Supervision, Funding acquisition, Review & editing.

Declaration of competing interest

The authors declare that they have no known competing financial interests or personal relationships that could have appeared to influence the work reported in this paper.

Data availability

Data will be made available on request.

References

[1] Chinnasamy V, Heo J, Jung S, Lee H, Cho H. Shape stabilized phase change materials based on different support structures for thermal energy storage applications–A review. Energy 2023:262. https://doi.org/10.1016/j.energy.2022.125463.
[2] Guo SY, Yan D, Hu S, An JJ. Global comparison of building energy use data within the context of climate change. Energy Build 2020;226:110362. https://doi.org/10.1016/j.enbuild.2020. ARTN 110362.
[3] Lizana J, Chacartegui R, Barrios-Padura A, Ortiz C. Advanced low-carbon energy measures based on thermal energy storage in buildings: a review. Renew Sustain Energy Rev 2018;82:3705–49. https://doi.org/10.1016/j.rser.2017.10.093.
[4] IEA. Building envelopes. Paris: IEA; 2021. https://www.iea.org/reports/building-envelopes.
[5] Liu C, Sun Y, Li N, Zhang B, Liu J. Improved energy utilization efficiency via adding solar radiant heating mode for traditional bioreactor to dispose straw: experimental and numerical evaluation. Waste Manag 2019;89:303–12. https://doi.org/10.1016/j.wasman.2019.04.027.
[6] Liu C, Sun Y, Li N, Zhang B, Zhen F. Impact of temperature fluctuation on anaerobic fermentation process of upgrading bioreactor under solar radiant heating. Appl Therm Eng 2019;156:382–91. https://doi.org/10.1016/j.applthermaleng.2019.04.092.
[7] Liu C, Sun Y, Yang F, Liu J. Effect of solar irradiance on photo biochemical transformation process of direct absorption methane digester. Energy Convers Manag 2018;172:173–84. https://doi.org/10.1016/j.enconman.2018.07.026.
[8] Meysam N, Mohamed J, Nasko T. Bio-based phase change materials incorporated in lignocellulose matrix for energy storage in buildings—a review. Energies 2020. https://doi.org/10.3390/en13123065.
[9] Zhang HL, Baeyens J, Degrève J, Cáceres G, Segal R, Pitié F. Latent heat storage with tubular-encapsulated phase change materials (PCMs). Energy 2014;76:66–72. https://doi.org/10.1016/j.energy.2014.03.067.
[10] Cai RN, Sun ZG, Yu H, Meng EL, Wang JQ, Dai ML. Review on optimization of phase change parameters in phase change material building envelopes. J Build Eng 2021;35. ARTN 10197910.1016/j.jobe.2020.101979.
[11] Marie D, Clément M, Stefania D, Jean-Luc D, Sergio S-M, Alexandre G, et al. Characterization of fatty acids as biobased organic materials for latent heat storage. Materials 2021. https://doi.org/10.3390/ma14164707.
[12] Liu C, Sun Y, Li D, Bian J, Wu Y, Li P, et al. Influence of enclosure filled with phase change material on photo-thermal regulation of direct absorption anaerobic reactor: numerical and experimental study. Appl Energy 2022;313. https://doi.org/10.1016/j.apenergy.2022.118885.
[13] Ikutegbe CA, Farid MM. Application of phase change material foam composites in the built environment: a critical review. Renew Sustain Energy Rev 2020:131. https://doi.org/10.1016/j.rser.2020.110008. ARTN 110008.
[14] Si W, Tingxian L, Minqiang W, Jiaxing X, Yihao H, Jingwei C, et al. Highly thermally conductive and flexible phase change composites enabled by polymer/graphite nanoplatelet-based dual networks for efficient thermal management. J Mater Chem 2020. https://doi.org/10.1039/d0ta05904h.
[15] Dimberu GA, Beom Yeol Y, Sungwoong Y, Hyeonseong Y, Seunghwan W, Sumin K. Structurally advanced hybrid support composite phase change materials: architectural synergy. Energy Storage Mater 2021. https://doi.org/10.1016/j.ensm.2021.07.022.
[16] Ke W, Ji J, Zhang C, Xie H, Tang Y, Wang C. Effects of the PCM layer position on the comprehensive performance of a built-middle PV-Trombe wall system for building application in the heating season. Energy 2023;267. https://doi.org/10.1016/j.energy.2022.126562.
[17] Duquesne M, Mailhé C, Ruiz-Onofre K, Achchaq F. Biosourced organic materials for latent heat storage: an economic and eco-friendly alternative. Energy 2019;188. https://doi.org/10.1016/j.energy.2019.116067.
[18] Tian Y, Liu A, Wang J, Zhou Y, Bao C, Xie H, et al. Optimized output electricity of thermoelectric generators by matching phase change material and thermoelectric material for intermittent heat sources. Energy 2021:233. https://doi.org/10.1016/j.energy.2021.121113.
[19] Jialu T, Jingde L, Yue L, Daoyu Q, Zheng Y, Xin K. Technology development and application prospects of organic-based phase change materials: an overview. Renew. Sustainable Energy Rev. 2022. https://doi.org/10.1016/j.rser.2022.112175.
[20] Yinxu Z, Xuelai Z, Weisan H. Review of preparation technologies of organic composite phase change materials in energy storage. J Mol Liq 2021. https://doi.org/10.1016/j.molliq.2021.115923.
[21] Samer K, Mary Anne W. Organic phase change materials for thermal energy storage: influence of molecular structure on properties. Molecules 2021. https://doi.org/10.3390/molecules26216635.

[22] Shaokun S, Tingting Z, Feng Q, Wanting Z, Taorui C, Yi G, et al. Natural microtubule encapsulated phase change material with high thermal energy storage capacity. Energy 2019. https://doi.org/10.1016/j.energy.2019.02.052.

[23] El-Raheim DA, Mohamed A, Abou-Ziyan H, Fatouh M. The essential properties governing the appropriate selection of phase change materials integrated into heavy structure buildings. Energy 2023:266. https://doi.org/10.1016/j.energy.2022.126515.

[24] António F, Romeu V, José L, Claudino C, Fernanda R, Jérôme K. Indoor thermal comfort assessment using different constructive solutions incorporating PCM. Appl Energy 2017. https://doi.org/10.1016/j.apenergy.2017.09.032.

[25] Zanshe W, Ran L, Juntao H, Xianwei H, Zhaolin G. Experimental study on hybrid organic phase change materials used for solar energy storage. J Therm Sci 2020. https://doi.org/10.1007/s11630-020-1224-3.

[26] Quanying Y, Xiangyu S. The thermal storage performance of mixtures consisting of liquid paraffin and fatty acids. Int J Sustain Energy 2017. https://doi.org/10.1080/14786451.2017.1323899.

[27] Hassan N, Mariah B, Majid A, Arunachala MK. Fatty acids based eutectic phase change system for thermal energy storage applications. Appl Therm Eng 2018. https://doi.org/10.1016/j.applthermaleng.2018.07.025.

[28] Samer K, Michel BJ, Ali CK, Dominic G, Mary Anne W. Stable, low-cost phase change material for building applications: the eutectic mixture of decanoic acid and tetradecanoic acid. Appl Energy 2016. https://doi.org/10.1016/j.apenergy.2016.01.115.

[29] Vennapusa Jagadeeswara R, Konala A, Prakhar D, Jitendra S, Sumit P, Sujay C. Thermal buffering performance evaluation of fatty acids blend/fatty alcohol based eutectic phase change material and simulation. J Energy Storage 2021. https://doi.org/10.1016/j.est.2021.102499.

[30] Zhanjiang H, Chaoming W, Wenbing J, Xiao L, Zhengyu C. Preparation and thermal properties of 1-hexadecanol-palmitic acid eutectic mixture/activated carbon composite phase change material for thermal energy storage. ChemistrySelect 2019. https://doi.org/10.1002/slct.201801773.

[31] Rohitash K, Sumita V, Ambesh D. Fatty acids/1-dodecanol binary eutectic phase change materials for low temperature solar thermal applications: design, development and thermal analysis. Sol Energy 2017. https://doi.org/10.1016/j.solener.2017.07.082.

[32] Jingyu H, Shilei L, Xiangfei K, Shangbao L, Yiran l. Form-stable phase change materials based on eutectic mixture of tetradecanol and fatty acids for building energy storage: preparation and performance analysis. Materials 2013. https://doi.org/10.3390/ma6104758.

[33] Cárdenas-Ramírez C, Gómez MA, Jaramillo F, Cardona AF, Fernández AG, Cabeza LF. Experimental steady-state and transient thermal performance of materials for thermal energy storage in building applications: from powder SS-PCMs to SS-PCM-based acrylic plaster. Energy 2022:250. https://doi.org/10.1016/j.energy.2022.123768.

[34] Jingtao L, Dahua J, Hua F, Yuzhen X, Zui Z, Weiliang Y. Preparation and energy storage properties of a lauric acid/octadecanol eutectic mixture. ACS Omega 2021. https://doi.org/10.1021/acsomega.1c03626.

[35] Jianguo Z, Weizhong L, Lindong W. Thermal properties of lauric acid/1-tetradecanol binary system for energy storage. Appl Therm Eng 2011. https://doi.org/10.1016/j.applthermaleng.2011.01.008.

[36] Hongguang Z, Jiaoqun Z, Weibing Z, Fengli L, Kang L. Synthesis and thermal properties of a capric acid-modified expanded vermiculite phase change material. J Mater Sci 2018. https://doi.org/10.1007/s10853-018-2988-7.

[37] Yuntao L, Hua Y, Qun W, Hongtao W, Yongbo H. Structure and thermal properties of decanoic acid/expanded graphite composite phase change materials. J Therm Anal Calorim 2017. https://doi.org/10.1007/s10973-016-6068-4.

[38] Jingwen Q, Yunkang C, Changlu X, Guiyin F. Synthesis and thermal properties of 1-octadecanol/nano-TiO2/carbon nanofiber composite phase change materials for thermal energy storage. Mater Chem Phys 2021. https://doi.org/10.1016/j.matchemphys.2021.125041.

[39] Zhou Q, Zhang Y, Guo HB, Li QH, Li DX. Research on the thermo physical properties of lauric acid-capric acid binary mixture phase change materials. In: Conference research on the thermo physical properties of lauric acid-capric acid binary mixture phase change materials, Shanghai, PR China. vols. 226–228. Trans Tech Publications Ltd; 2012. p. 1704.

[40] Karolina M, Vijayaraghavan R, Mega K, Douglas RM. Role of hydrogen bonding in phase change materials. Crystal Growth & Design; 2020. https://doi.org/10.1021/acs.cgd.9b01541.

[41] Samer K, Mary Anne W. Prediction of the properties of eutectic fatty acid phase change materials. Thermochim Acta 2018. https://doi.org/10.1016/j.tca.2017.12.024.

[42] Rostami S, Afrand M, Shahsavar A, Sheikholeslami M, Kalbasi R, Aghakhani S, et al. A review of melting and freezing processes of PCM/Nano-PCM and their application in energy storage. Energy 2020. https://doi.org/10.1016/j.energy.2020.118698.

[43] David D, Johannes K, Kuznik F. Quantification of the natural convection perturbations on differential scanning calorimetry measurements of PCMs. Thermochim Acta 2017. https://doi.org/10.1016/j.tca.2017.06.004.

[44] Sun X, Zhang Q, Medina MA, Lee KO. Experimental observations on the heat transfer enhancement caused by natural convection during melting of solid–liquid phase change materials (PCMs). Appl Energy 2015. https://doi.org/10.1016/j.apenergy.2015.03.078.

[45] Fatahi H, Claverie J, Poncet S. Experimental investigation of the rheological and phase change behavior of adipic acid as a phase change material (PCM) for thermal energy storage at 150 °C. Thermochim Acta 2022:711. https://doi.org/10.1016/j.tca.2022.179206.

[46] Li L, Yu H, Wang X, Zheng S. Thermal analysis of melting and freezing processes of phase change materials (PCMs) based on dynamic DSC test. Energy Build 2016. https://doi.org/10.1016/j.enbuild.2016.08.058.

[47] Feng G, Huang K, Xie H, Li H, Liu X, Liu S, et al. DSC test error of phase change material (PCM) and its influence on the simulation of the PCM floor. Renew Energy 2016. https://doi.org/10.1016/j.renene.2015.07.085.

[48] Wengshi F. Fourier transform infrared spectroscopy analysis. Chemical Industry Press; 2016.

[49] Weirong Han, Shubing Liu ZZ, Chang Yongfang, Hu Ruisheng. Hongwei Yu Study on structure and phase transformation mechanism of stearic acid by variable temperature Fourier transform infrared spectroscopy. Phy. Chem. Anal. (Chemical Volume) 2014:50.

[50] Weng Manyahui WW. Temperature-variable infrared spectroscopy analysis of the phase transition process of organic phase change materials. In: The 11th national annual conference of applied chemistry 2009. Guilin; 2009.

[51] Pielichowska K, Głowinkowski S, Lekki J, Biniaś D, Pielichowski K, Jenczyk J. PEO/fatty acid blends for thermal energy storage materials. Structural/morphological features and hydrogen interactions. Eur Polym J 2008. https://doi.org/10.1016/j.eurpolymj.2008.07.047.

[52] Linnan Du YW, Zhou Guanlin, Ruo Ruobing, Hu Mengxuan, Liu Haiyue. Study on infrared and variable temperature infrared spectra of Sodium carboxymethyl cellulose. Coal and Chemical Industry 2009;42.

[53] Jian-Jun Z, Jian-Ling Z, Shu-Mei H, Ke-Zhong W, Xiao-Di L. Thermal studies on the solid–liquid phase transition in binary systems of fatty acids. Thermochim Acta 2001. https://doi.org/10.1016/s0040-6031(00)00766-8.

[54] Xiaowu Wang HX. Study on solid-solid phase transition mechanism of polyols. Acta Phys Sin 2011;60.

[55] Victor AL-F. Infrared difference spectroscopy of proteins: from bands to bonds. Chem Rev 2020. https://doi.org/10.1021/acs.chemrev.9b00449.

[56] Antonio P, Fernanda P, Edmund DC, Alejandro GM, Giuseppe M. Molecular insights into the eutectic tripalmitin/tristearin binary system. J Am Chem Soc 2018. https://doi.org/10.1021/jacs.8b04729.

[57] Lubensky Socolar, Steinhardt Bancel, Heiney. Distortion and peak broadening in quasicrystal diffraction patterns. Phys Rev Lett 1986. https://doi.org/10.1103/physrevlett.57.1440.

[58] Fan Z, Zhao Y, Liu X, Shi Y, Jiang D. Thermal properties and reliabilities of myristic acid-paraffin wax binary eutectic mixture as a phase change material for solar energy storage. RSC Adv 2022;12(20):12303–9. https://doi.org/10.1039/d1ra09238c.

[59] Dimberu GA, Wenjun D, Xiubing H, Hongyi G, Ge W. Introduction of organic-organic eutectic PCM in mesoporous N-doped carbons for enhanced thermal conductivity and energy storage capacity. Appl Energy 2017. https://doi.org/10.1016/j.apenergy.2017.12.025.

[60] Fan Z, Zhao Y, Liu X, Shi Y, Jiang D. Thermal properties and reliabilities of lauric acid-based binary eutectic fatty acid as a phase change material for building energy conservation. ACS Omega 2022. https://doi.org/10.1021/acsomega.2c01420.

[61] Philip N, Raam Dheep G, Sreekumar A. Cold thermal energy storage with lauryl alcohol and cetyl alcohol eutectic mixture: thermophysical studies and experimental investigation. J Energy Storage 2020;27. https://doi.org/10.1016/j.est.2019.101060.